Sensor networks

On the Performance of Cache- and Energy Harvesting-Assisted NOMA in D2D Communications With Hardware Impairments

Alok K. Shukla[1,2*], Jules M. Mouale[2**], Prabhat Kumar Upadhyay[1**], Fambirai Takawira[2**], and Pedro H. Juliano Nardelli[3**]

[1] Department of Electrical Engineering, Indian Institute of Technology Indore, Indore, Madhya Pradesh 453552, India
[2] School of Electrical, Information Engineering, University of the Witwatersrand, Johannesburg 2001, South Africa
[3] School of Energy Systems, Lappeenranta-Lahti University of Technology, 53850 Lappeenranta, Finland
[*] Graduate Student Member, IEEE
[**] Senior Member, IEEE

Manuscript received 16 August 2023; accepted 24 August 2023. Date of publication 5 September 2023; date of current version 10 October 2023.

Abstract—In this letter, we investigate a cache- and energy harvesting (EH)-enabled device-to-device (D2D)- aided nonorthogonal multiple access (NOMA) network with hardware impairments at the transceiver nodes. Considering imperfect successive interference cancellation at the legitimate users, we derive the analytical expressions of the outage probability (OP) for both a cache-free (CF) and a cache-aided (CA) relaying system. In addition, the asymptotic behavior of the proposed scheme is studied in order to get further insights on the impact of the system parameters. Extensive Monte Carlo simulations reveal the superiority of the proposed scheme over the CF relaying system, and are shown to validate the accuracy of the derived analytical framework.

Index Terms—Sensor networks, caching, device-to-device (D2D), energy harvesting (EH), nonorthogonal multiple access (NOMA), outage probability (OP).

I. INTRODUCTION

Future wireless networks are expected to face significant challenges because of the rapid growth of intelligent applications that place stringent requirements on spectral efficiency (SE), energy efficiency, and latency. The synergy of wireless caching and nonorthogonal multiple access (NOMA) (see [1] and [2]) has resulted in an improved SE and network coverage. Specifically, the authors in [1] investigated the coverage probability by exploiting stochastic geometry, whereas the authors in [2] designed two NOMA-based caching schemes, namely the push-then-deliver and the push-and-deliver schemes and subsequently examined the outage probability (OP) and cache hit probability.

Meanwhile, the energy limitations of battery-operated devices are another challenge for the design of futuristic communication networks. To this end, energy harvesting (EH) through a radio frequency (RF) signal is one of the promising technologies to power the wireless network. The joint study of EH and wireless caching has been done in [3] and [4]. Specifically, a device-to-device (D2D) network was proposed in [3], wherein each mobile user (MU) is assisted with a cache storage and an EH-circuitry. The authors proposed a content delivery strategy and categorized the MUs into three modes, namely self-satisfied, D2D communication, and cellular communication, taking into account the file's popularity and the energy limitation. Gautam et al. [4] examined two maximization problems, namely the relay-destination throughput maximization and the energy stored maximization, and presented the relay selection and power allocation algorithms, respectively, for the cache- and EH-assisted relay transmission. However, to the best of the authors' knowledge, the amalgamation of EH, NOMA, and wireless caching is still in its infancy. Recently, Ren et al. [5] proposed simultaneous wireless information and power transfer (SWIPT)-enabled wireless caching networks with NOMA and evaluated the performance by optimizing both the power and time allocation factors. It is noteworthy that most of the reported studies either addressed an EH structure with a separate energy source or assumed the EH to be a separate entity from caching. Recently, the work of [6] has tackled the mathematical intractability of an EH-based cognitive NOMA system through a deep learning approach. However, wireless caching is not considered in that work, let alone the practical issues of hardware impairments (HIs).[1]

Motivated by the preceding discussion, we propose novel EH-assisted D2D-aided NOMA network with hardware impairments and wireless caching, where a cache-enabled power splitting (PS)-based receiver architecture is employed at the near user (NU) to act as a decode-and-forward (DF) relay. The main contributions of this letter are summarized as follows. 1) We derive the OP expressions of all the users considering HIs and imperfect successive interference cancellation (ipSIC). To get useful insights for the considered system, we evaluate the cache hit probability using the derived expressions of the OP. In addition, the asymptotic behavior of the proposed system is studied to assess the impact of the various parameters on the proposed system. 2) A comparison between a cache-aided (CA) relaying scheme and its cache-free (CF) counterpart is carried out wherein the superiority of the former over the latter is illustrated.

The rest of this letter is organized as follows. Section II presents the system model. Section III shows the performance analysis. In Section IV, numerical and simulation results are discussed. Finally, Section V concludes this letter.

II. SYSTEM MODEL

As shown in Fig. 1, we consider an EH-assisted D2D-aided NOMA network with wireless caching consisting of a base station (BS) node P, two NUs (D_1 as node R and D_{11} as node Q), and a far user (FU) (D_2 as

Corresponding authors: Jules M. Moualeu; Pedro H. J. Nardelli. (e-mail: jules.moualeu@wits.ac.za; pedro.nardelli@lut.fi)
Associate Editor: Francisco Falcone.
Digital Object Identifier 10.1109/LSENS.2023.3310354

[1] In practical RF transmissions, the transceivers may be subjected to hardware distortions as a result of the I/Q imbalances, phase noises, and amplifier nonlinearities [13]

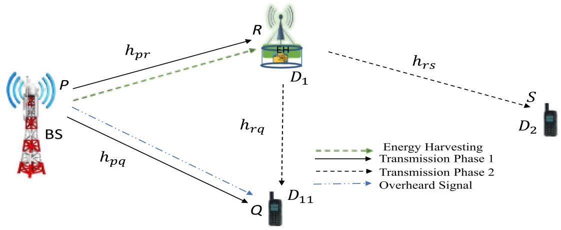

Fig. 1. System model.

node S) over Rayleigh fading.[2] Herein, node R acts as a PS-based EH DF relay [12] with caching capacity and cooperates by forwarding the intended information received from BS to node S. However, there is no direct communication between BS and FU D_2 due to heavy shadowing and long distance. All the nodes are assumed to be equipped with a single antenna. Due to the energy restriction on node R, it first harvests energy from the signal emanating from node P and then splits the corresponding received power to relay the information of FU D_2 and to transmit D_{11} signal.

The channel coefficient between any two nodes i and j is denoted by $h_{ij} \sim \mathcal{CN}(0, \lambda_{ij})$, with zero mean and variance λ_{ij}, where $\lambda_{ij} = d_{ij}^{-\nu}$, $i \in (p, r)$, $j \in (q, r, s)$, $i \neq j$, and ν and d_{ij} denote the pathloss exponent and the normalized distance, respectively. Under statistical channel state information, it is assumed that the average channel powers associated with links $i \to j$, are ordered as $\lambda_{rq} > \lambda_{pr} \approx \lambda_{pq} > \lambda_{pr} > \lambda_{rs}$, without loss of generality [7]. It is assumed that all the receiving nodes are subjected to additive white Gaussian noise (AWGN), defined as $\mathcal{CN}(0, \sigma^2)$ with σ^2 being the noise variance. The probability density function and the cumulative distribution function of an exponential random variable $Z \triangleq |h_{ij}|^2$ with mean λ_{ij} are given by $f_Z(z) = \frac{1}{\lambda_{ij}} \exp(\frac{-z}{\lambda_{ij}})$ and $F_Z(z) = 1 - \exp(\frac{-z}{\lambda_{ij}})$, respectively, where $z \geq 0$.

A. Caching Model

The content files are classified into active files and proactive files based on distinct needs. In other words, an active file is defined as a file that the user is presently requesting, and a proactive file is a file that the user is not requesting at the moment but in future [10]. Therefore, when BS broadcasts the information, the received signal at node P pushes the active files for D_1 and stores the proactive files of D_2. The active and proactive content files are stored in a finite content library denoted by $F_a = \{f_{a_1}, f_{a_2}, \ldots, f_{a_N}\}$ and $F_p = \{f_{p_1}, f_{p_2}, \ldots, f_{p_M}\}$, respectively, where, N and M denotes the number of active and proactive files. Following the most popular content-based caching scheme [10], node R can cache up to C files during the content pushing phase out of the M total content files ($C < M$) of the library at BS. Moreover, based on the statistical property of the Zipf distribution, the probabilities of requesting the mth most popular files $f_{p_M}(1 \leq m \leq M)$ can be given as [3] $P(f_{p_M}) = (m^{\chi} \sum_{i=1}^{M} i^{-\chi})^{-1}$ with $\chi > 0$ as the shape parameter denoting the content popularity skewness. The overall communication in the proposed system model occurs in the two information processing (IP) phases over a transmission block of duration T as described in the following.

B. IP Phase-1

During IP Phase-1 of duration $T/2$ (denoted by t_1), BS node P broadcasts the superimposed signal $X_P = \sum_{j=1}^{2} \sqrt{\delta_j P_p} x_j + \eta_{tp}$ toward node R, which is overheard by node Q. Here, P_p denotes the BS transmit power, x_j is the intended signal for D_j, δ_j is the power allocation factor, $j \in (1, 2)$, with $\sum_{j=1}^{2} \delta_j = 1$, $\delta_2 > \delta_1$, and $\eta_{\text{tp}} \sim \mathcal{CN}(0, \Omega_{\text{tp}}^2 P_p)$ is the distortion noise with Ω_{tp} being the level of impairment at node P. Thus, the signal received at node R can be given by $y_{pr}^{t_1} = h_{pr} X_P + \eta_{rD_1} + \vartheta_{pr}$, where $\eta_{rD_1} \sim \mathcal{CN}(0, \Omega_{rD_1}^2 P_p |h_{pr}|^2)$ is the distortion noise with Ω_{rD_1} being the level of impairment at node R, and ϑ_{pr} denotes the AWGN variable. Herein, node R bifurcates the received signal as $\sqrt{\beta} y_{pr}^{t_1}$ for EH and $\sqrt{(1-\beta)} y_{pr}^{t_1}$ for information transmission, where $0 \leq \beta \leq 1$ represents the PS factor. The received signal for EH at node R is written as $\sqrt{\beta} y_{pr}^{t_1} = \sqrt{\beta}(h_{pr} X_P + \eta_{rD_1} + \vartheta_{pr})$. Thus, the energy harvested at node R is given by $E_h = \beta \mu (P_p \delta_1 + P_p \delta_2) |h_{pr}|^2 \frac{T}{2} = \beta \mu P_p |h_{pr}|^2 \frac{T}{2}$, where μ $(0 < \mu \leq 1)$ indicates the energy conversion efficiency. Note that HIs are omitted because all nonideal factors can be encompassed in μ [11]. Thus, the transmit power of node R for the remaining $\frac{T}{2}$ period can be given by $P_r = \frac{E_h}{T/2} = \beta \mu |h_{pr}|^2 P_p$. The received base-band signal at node R is given by $\sqrt{(1-\beta)} y_{pr}^{t_1} = \sqrt{(1-\beta)} h_{pr} X_P + \eta_{rD_1} + N_{pr}$, where $N_{pr} = \sqrt{(1-\beta)} \vartheta_{pr} + \vartheta_{\text{RF}}$, and ϑ_{RF} is the sampled AWGN due to RF to base-band signal conversion.

Following the NOMA principle, node R first decodes signal x_2 treating x_1 as noise, and then applies successive interference cancellation (SIC) to decode signal x_1. Thus, the signal-to-interference-plus-noise ratios (SINRs) at node R to decode x_2 and x_1, respectively, can be given by

$$\gamma_{pr}^{x_2, t_1} = (1-\beta)\delta_2 \gamma_{pr} / \left(\mathcal{A}_1 \gamma_{pr} + 1\right) \tag{1}$$

$$\gamma_{pr}^{x_1, t_1} = (1-\beta)\delta_1 \gamma_{pr} / \left(\mathcal{A}_2 \gamma_{pr} + 1\right) \tag{2}$$

where $\gamma_{pr} = \rho_p h_{pr}$ with $\rho_p = P_p/\sigma^2$ denoting the transmit signal-to-noise ratio (SNR), $\mathcal{A}_1 = \delta_1 + \Omega_{pr}^2$, $\mathcal{A}_2 = \tau_1 \delta_2 + \Omega_{pr}^2$, $\Omega_{pr} = \sqrt{\Omega_{tp}^2 + \Omega_{rD_1}^2}$, and τ_1 $(0 \leq \tau_1 \leq 1)$ being the residual interference (RI) parameter; $\tau_1 = 0$ denotes the perfect SIC (pSIC) case. Moreover, the signal broadcast by BS is overheard by node Q and then decodes the stronger signal x_2 while considering the weak signal x_1 as noise. Thus, the received SINR at node Q can be computed by

$$\gamma_{pq}^{x_2, t_1} = \delta_2 \gamma_{pq} / (\mathcal{A}_3 \gamma_{pq} + 1) \tag{3}$$

where $\gamma_{pq} = \rho_p h_{pq}$, $\mathcal{A}_3 = \delta_1 + \Omega_{pq}^2$, and $\Omega_{pq} = \sqrt{\Omega_{tp}^2 + \Omega_{rq}^2}$, with Ω_{rq} denoting the level of impairment at node Q.

C. IP Phase-2

In the next $T/2$ time period (denoted by t_2), upon successful decoding of x_2 at node R, it transmits the superimposed signal $X_R = \sqrt{\delta_3 P_r} x_2 + \sqrt{\delta_{11} P_r} x_{11} + \eta_{tr}$, where x_2 and x_{11} are intended signals for S and Q, respectively, $\eta_{tr} \sim \mathcal{CN}(0, \Omega_{tr}^2 P_r)$ is the distortion noise with Ω_{tr} being the level of impairment at node R, and δ_3 and δ_{11} are the PAFs. Here, we assume that $d_{rs} > d_{rq}$, yielding $\delta_3 > \delta_{11}$ with $\delta_3 + \delta_{11} = 1$. Thus, the received signal at node S can be expressed as $y_{rs}^{t_2} = h_{rs} X_R + \eta_{rD_2} \eta_{rD_2} + \vartheta_{rs}$, where ϑ_{rs} is the AWGN variable and $\eta_{rD_2} \sim \mathcal{CN}(0, \Omega_{rD_2}^2 P_r |h_{rs}|^2)$ is the distortion noise with Ω_{rD_2} being the level of impairment at node S. The received SINR to decode x_2 at node S is given by

$$\gamma_{rs}^{x_2, t_2} = \frac{\delta_3 \beta \mu \gamma_{pr} |h_{rs}|^2}{\beta \mu \gamma_{pr} |h_{rs}|^2 \mathcal{A}_4 + 1} \tag{4}$$

where $\mathcal{A}_4 = \delta_{11} + \Omega_{rs}^2$ with $\Omega_{rs} = \sqrt{\Omega_{tr}^2 + \Omega_{rD_2}^2}$.

In order to maximize the spectrum utilization, P simultaneously transmits the new signal $\hat{x}_1$ to node Q with transmit power $\sqrt{\delta_1^* P_p}$, for $\delta_1^* \in (0, 1)$, during the second phase. However, during the second phase transmission, Q receives a composite signal X_R which can be estimated and partially eliminated by using the received information of x_2 during IP phase-1. Therefore, the received signal during the second phase at node Q is given by $y_{pq}^{t_2} = (h_{pq}(\sqrt{\delta_{11}^* P_p} \hat{x}_1 + \eta_{tp}) + \eta_{rq}) + (h_{rq} X_R +$

[2]The adoption of the D2D communication is motivated by the fact that in typical 5G application scenarios, such as massive machine-type communications and the Internet of Things, "users" may be low-cost sensors deployed in small geographical areas, where both LOS and/or non-LOS exist, which can be better modeled by the Rician fading channel. However, most of the existing D2D-aided cooperative NOMA-based literature [8], [9] mainly consider the Rayleigh fading channel which is reasonable and suitable for rich scattering scenarios without LOS, and for its simplicity in typical cellular situations. The obtained results pertaining to our proposed work would serve as a benchmark for future works that will consider more general fading distributions.

$\eta_{rq}) + \vartheta_{pq}$, where $\eta_{rq} \sim \mathcal{CN}(0, \Omega_{rq}^2 P_p |h_{rq}|^2)$ is the distortion noise with Ω_{rq} being the level of impairment at node S. Hereby, node Q first decodes x_{11} by considering $\hat{x}_1$ as noise and then perform SIC to decode its own signal. Thus, the received SINR at node Q to decode x_{11} and $\hat{x}_1$, respectively, can be given by

$$\gamma_{pq}^{x_{11},t_2} = \frac{\delta_{11}\beta\mu\gamma_{pr}|h_{rq}|^2}{\gamma_{pq}\mathcal{A}_5 + \beta\mu\gamma pr|h_{rq}|^2\Omega_{rq}^2 + 1} \tag{5}$$

$$\gamma_{pq}^{\hat{x}_1,t_2} = \frac{\delta_1^*\gamma_{pq}}{\gamma_{pq}\Omega_{pq}^2 + \gamma_{pr}|h_{rq}|^2\mathcal{A}_6 + 1} \tag{6}$$

where $\mathcal{A}_5 = \delta_1^* + \Omega_{pq}^2$, $\mathcal{A}_6 = \beta\mu(\delta_{11}\tau_2 + \Omega_{D_{11}}^2)$, $\Omega_{D_{11}} = \sqrt{\Omega_{tq}^2 + \Omega_{rq}^2}$, τ_2 $(0 \le \tau_1 \le 1)$ is the RI parameter, and $\tau_1 = 0$ denotes the pSIC case.

III. PERFORMANCE ANALYSIS

In this section, we comprehensively analyze the performance of the CF/CA EH-assisted D2D-aided NOMA network in terms of OP and cache hit probability. Moreover, we also derive the asymptotic expressions for the OP to get additional insights. For this, we consider the target data rates as r_1, r_2, and r_{11} for D_1, D_2, and D_{11}, respectively.

A. CF Scheme

1) OP of NU D_1: The NU D_1 is said to be in outage if it is unable to decode either of the symbols x_1 or x_2. Therefore, the OP expression for D_1 can be obtained as

$$P_{\text{out},D_1}^{t_1} = 1 - \Pr\left[\gamma_{pr}^{x_2,t_1} > R_2^{\text{th}}, \gamma_{pr}^{x_1,t_1} > R_1^{\text{th}}\right] \tag{7}$$

where $R_1^{\text{th}} = 2^{2r_1} - 1$ and $R_2^{\text{th}} = 2^{2r_2} - 1$. By making use of the involved SINRs from (1) and (2) in (7), and performing some algebraic manipulations, $P_{\text{out},D_1}^{t_1}$ can be expressed as

$$P_{\text{out},D_1}^{t_1} = 1 - \Pr\left[|h_{pr}|^2 > \max\{\mathcal{B}_0, \mathcal{B}_1\}/\rho_p\right] \tag{8}$$

where $\mathcal{B}_0 = \frac{R_2^{\text{th}}}{\delta_2 - \mathcal{A}_1 R_2^{\text{th}}}$ and $\mathcal{B}_1 = \frac{R_1^{\text{th}}}{\delta_1 - \mathcal{A}_2 R_1^{\text{th}}}$. Under the conditions $\delta_2 > \mathcal{A}_1 R_2^{\text{th}}$ and $\delta_1 > \mathcal{A}_2 R_1^{\text{th}}$, (8) is further evaluated as $P_{\text{out},D_1}^{t_1} = 1 - e^{\left(\frac{-\Delta_1}{\lambda_{pr}\rho_p}\right)}$, where $\Delta_1 \triangleq \max\{\mathcal{B}_0, \mathcal{B}_1\}$. The asymptotic expression for $P_{\text{out},D_1}^{t_1}$ at high SNR ($\rho_p \to \infty$) can be deduced by making use of approximation $e^{-x} \simeq 1 - x$ for small x to get

$$P_{\text{out},D_1}^{t_1,asy} = \Delta_1/\lambda_{pr}\rho_p. \tag{9}$$

2) OP of NU D_{11}: The OP for D_{11} can be formulated as

$$P_{\text{out},D_{11}}^{t_2} = 1 - \Pr\left[\gamma_{pq}^{x_2,t_1} > R_2^{\text{th}}, \gamma_{pq}^{x_{11},t_2} > R_2^{\text{th}}, \gamma_{pq}^{\hat{x}_1,t_2} > R_{11}^{\text{th}}\right] \tag{10}$$

where $R_{11}^{\text{th}} = 2^{2r_{11}} - 1$. By substituting the associated SINRs from (3), (5), and (6) in (10), and through some algebraic manipulations, $P_{\text{out},D_{11}}$ can be reexpressed as

$$\begin{aligned} P_{\text{out},D_{11}}^{t_2} &= 1 - \Pr\left[Z > \mathcal{B}_2/\rho_p\right] \\ &\quad \times \Pr\left[Z < \mathcal{B}_3 XY - \mathcal{B}_4, Z > \mathcal{B}_5 + \mathcal{B}_6 XY\right] \end{aligned} \tag{11}$$

where $Z \triangleq |h_{pq}|^2$, $X \triangleq |h_{pr}|^2$, $Y \triangleq |h_{rq}|^2$, $\mathcal{B}_2 = R_2^{\text{th}}/(\delta_1 - \mathcal{A}_3 R_2^{\text{th}})$, $\mathcal{B}_3 = \frac{\beta\mu(\delta_{11} - \Omega_{pq}^2 R_{11}^{\text{th}})}{\mathcal{A}_5 R_{11}^{\text{th}}}$, $\mathcal{B}_4 = \frac{1}{\rho_p \mathcal{A}_5}$, $\mathcal{B}_5 = \frac{R_{11}^{\text{th}}}{\rho_p(\delta_1 - \Omega_{pq}^2 R_{11}^{\text{th}})}$, and $\mathcal{B}_6 = \rho_p \mathcal{A}_6 \mathcal{B}_5$. The OP $P_{\text{out},D_{11}}$ in (11) can be further evaluated through the following theorem.

Theorem 1: Under the conditions $\delta_1 > (\mathcal{A}_3 R_2^{\text{th}} \cap \Omega_{pq}^2 R_{11}^{\text{th}})$ and $\delta_{11} > \Omega_{pq}^2 R_{11}^{\text{th}}$, $P_{\text{out},D_{11}}^{t_2}$ in (11) yields

$$P_{\text{out},D_{11}} = 1 - e^{\left(-\frac{\mathcal{B}_2}{\rho_p\lambda_{pq}}\right)}(\mathcal{P}_1 - \mathcal{P}_2) \tag{12}$$

where $\mathcal{P}_1$ and $\mathcal{P}_2$ can be given by

$$\mathcal{P}_1 = 1 - \frac{\lambda_{pq}}{\lambda_{rq}}\int_0^\infty \frac{e^{\left(-\frac{\mathcal{B}_4}{\lambda_{pr}\mathcal{B}_3 y} - \frac{y}{\lambda_{rq}}\right)}}{\lambda_{pr}\mathcal{B}_3 y + \lambda_{pq}} dy \tag{13}$$

$$\mathcal{P}_2 = 1 + \frac{\lambda_{pq}}{\lambda_{pr}\lambda_{rq}\mathcal{B}_6} e^{\left(\frac{-\mathcal{B}_5}{\lambda_{pq}} + \frac{\lambda_{pq}}{\lambda_{pr}\lambda_{rq}\mathcal{B}_6}\right)} \mathrm{E}_1\left(\frac{\lambda_{pq}}{\lambda_{pr}\lambda_{rq}\mathcal{B}_6}\right) \tag{14}$$

where $\mathrm{E}_1(\cdot)$ is the first-order exponential integral function [15, Eq. 5.1.1].

Proof: Follow the similar line of steps as used to derive [6, App. A]. ∎

Although the expression in (13) is given in a single-integral form, it can be computed effectively using mathematical software, such as Mathematica or Maple, and does so in a lot less time than the Monte Carlo simulation method. Moreover, the asymptotic expression for the OP of D_{11} at high SNR can be deduced by approximating the involved SINRs in (10) as $\gamma_{pq}^{x_{11},t_2} \approx \frac{\delta_{11}\beta\mu\gamma_{pr}|h_{rq}|^2}{\gamma_{pq}\mathcal{A}_5 + \beta\mu\gamma_{pr}|h_{rq}|^2\Omega_{rq}^2}$ and $\gamma_{pq}^{\hat{x}_1,t_2} \approx \frac{\delta_1^*\gamma_{pq}}{\gamma_{pq}\Omega_{pq}^2 + \gamma_{pr}|h_{rq}|^2\mathcal{A}_6}$ and making use of approximation $e^{-x} \simeq 1 - x$ for $x \to 0$. It can be given by

$$P_{\text{out},D_{11}}^{t_2,asy} = 1 - \left(1 - \frac{\mathcal{B}_2}{\rho_p\lambda_{pq}}\right)\frac{(\mathcal{B}_6 - \mathcal{B}_3)\lambda_{pr}\lambda_{rq}}{\lambda_{pq}}. \tag{15}$$

3) OP of FU D_2: For D_2, the outage occurs either when node R is unable to detect the symbol x_2 or when node S is unable to detect any symbol in conjunction with the successful detection of x_2 at node R. Therefore, the OP expression for D_2 can be expressed as

$$P_{\text{out},D_2}^{t_2} = \Pr\left[\gamma_{pr}^{x_2,t_1} < R_2^{\text{th}}\right] + \Pr\left[\gamma_{pr}^{x_2,t_1} \ge R_2^{\text{th}}, \gamma_{rs}^{x_2,t_2} < R_2^{\text{th}}\right]. \tag{16}$$

By invoking the respective SINRs in (16) with some mathematical rearrangement, $P_{\text{out},D_2}^{t_2}$ can be reexpressed as

$$P_{\text{out},D_2}^{t_2} = \Pr\left[X < \frac{\mathcal{B}_0}{\rho_p}\right] + \Pr\left[X \ge \frac{\mathcal{B}_0}{\rho_p}, V \le \frac{\mathcal{B}_7}{X\rho_p}\right] \tag{17}$$

where $X \triangleq |h_{pr}|^2$, $V \triangleq |h_{rs}|^2$, and $\mathcal{B}_7 = \frac{R_2^{\text{th}}}{\beta\mu(\delta_2 - \mathcal{A}_4 R_2^{\text{th}})}$. Further, $P_{\text{out},D_2}^{t_2}$ in (17) can be analytically evaluated under the conditions $\delta_2 > \mathcal{A}_4 R_2^{\text{th}}$ and $\delta_2 > \mathcal{A}_1 R_2^{\text{th}}$ as given in the following theorem.

Theorem 2: The analytical expression for $P_{\text{out},D_2}^{t_2}$ over Rayleigh fading channel can be obtained as

$$P_{\text{out},D_2}^{t_2} = 1 - \sum_{l=0}^{\infty}\frac{(-1)^l}{l!}\left(\frac{\mathcal{B}_7}{\lambda_{rs}\rho_p}\right)^l \frac{1}{\lambda_{rs}}\left(\frac{\mathcal{B}_0}{\rho_p}\right)^{1-l}\mathrm{E}_l\left(\frac{\mathcal{B}_0}{\lambda_{rs}\rho_p}\right) \tag{18}$$

where $\mathrm{E}_l(\cdot)$ is the lth order exponential integral function [15, Eq. 5.1.1].

Proof: By following the similar steps as used to derive [6, Appendix B], one can derive the expressions in (18). ∎

Remarks : Although the OP expression in (18) contains an infinite series, numerical results reveal that it swiftly converges to the exact solution with only the first 60 terms.

Further, by making use of approximation $e^{-x} \simeq 1 - x$ for small x and following the similar steps used to derive (18) in [6, Appendix B], the asymptotic expression for $P_{\text{out},D_2}^{t_2}$ at high SNR can be obtained as

$$P_{\text{out},D_2}^{t_2,asy} = \frac{\mathcal{B}_0}{\lambda_{pr}\rho_p} + \left(\frac{\mathcal{B}_7}{\lambda_{rs}\lambda_{pr}\rho_p}\right)\mathrm{E}_1\left(\frac{\mathcal{B}_0}{\lambda_{rs}\rho_p}\right). \tag{19}$$

B. CA Scheme

For the CA scheme, the OP of users D_{11} and D_2 can be given by $P_{\text{out},q}^{t_2,\text{CA}} = \sum_{i=1}^{C} P(f_{p_m}) P_{\text{out},q}^{t_2}$, where $q \in \{D_{11}, D_2\}$. Similarly, the asymptotic expression for the OP of the proposed CA scheme is given by

$$P_{\text{out},q}^{t_2,asy,\text{CA}} = \sum_{i=1}^{C} P(f_{p_m}) P_{\text{out},q}^{t_2,asy}. \tag{20}$$

C. Cache Hit Probability

The cache hit probability is defined as the probability that the file requested by a user (D_2 and D_{11}) is found at the local cache of node R

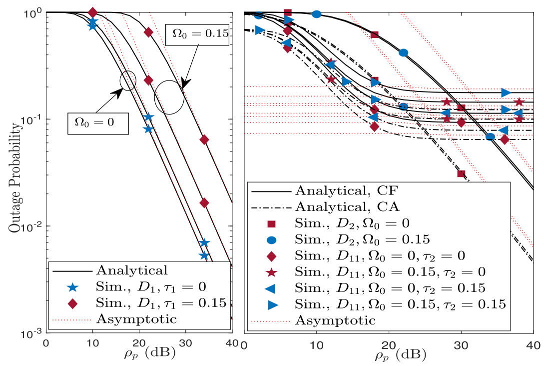

Fig. 2. OP of D_1, D_2, and D_{11} versus SNR.

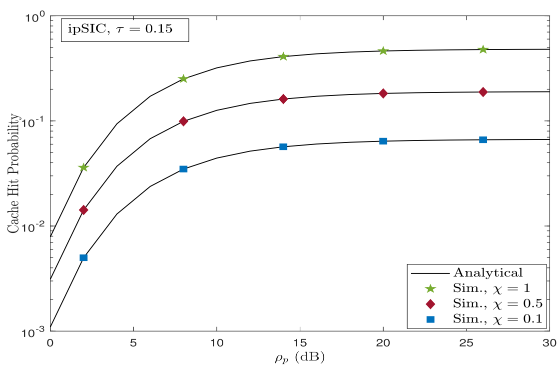

Fig. 3. Cache hit probability versus SNR.

and can be deduced as

$$P_{\text{out},D_1}^{\text{hit}} = \sum_{i=1}^{C} P(f_{p_m}) \left(1 - P_{\text{out},D_1}^{t_1}\right). \quad (21)$$

IV. NUMERICAL AND SIMULATION RESULTS

Without the loss of generality, we set $\delta_1 = 0.15$, $\delta_3 = 0.6$, $\alpha_{11}^* = 0.15$, $\beta = 0.2$, $\mu = 0.7$, $\chi = 2$, $M = 100$, $C = 20$, and $\sigma^2 = 1$. Furthermore, we set $\Omega_{\text{tp}} = \Omega_{rD_1} = \Omega_{rq} = \Omega_{tr} = \Omega_{rD_2} = \Omega_{rq} = \Omega_0$ as the level of HIs such that $\Omega_{pr} = \Omega_{rs} = \Omega_{D_{11}} = 2\sqrt{\Omega_0}$. These parameters are determined as the error vector magnitudes. Considering the 2-D (x, y) plane, the positions of nodes P, Q, R, and S are given, respectively, as follows: (0,0), (0.5, −0.5), (0.5, 0.5), (2, 0), and (−0.2, −0.45), respectively. The pathloss model is adopted, i.e., $\lambda_{ij} = d_{ij}^{-\nu}$ with pathloss exponent $\nu = 3$.

Fig. 2 shows the OP performance versus transmit SNR (ρ_p) for users D_1, D_2, and D_{11} under the pSIC and ipSIC cases. Herein, we set the parameters as $r_1 = r_2 = r_{11} = 0.5$ bps/Hz with HI levels $\Omega_0 = \{0, 0.15\}$ and SIC levels $\tau_1 = \tau_2 = \{0, 0.15\}$. It can be observed that an increase in the level of RI parameter yields a deterioration of the performance of D_1 and D_{11}. This is an indication that the decoding capability of D_1 and D_{11} decreases with an increase in the ipSIC level. Moreover, an increment in HI levels worsens the outage performance, which is evident from the pertinent curves. In addition, we compare the outage performances for the CA and the CF relay schemes of the proposed system. The obtained results show the superiority of the former scheme over the latter one, which is due to the effective use of caching at the relay node leading to the decrease of the transmission load and the optimization of the link performance. Furthermore, the asymptotic curves attained from derived expressions (for all the users) and the corresponding simulated ones overlap in the high-SNR regions, which validates the proposed asymptotic analysis.

Fig. 3 shows the variation in cache hit probability with respect to transmit SNR (ρ_p) with distinct content popularity parameter χ. It can be observed that the cache hit probability increases with increase in χ from 0.1 to 1, which is obvious because higher χ corresponds to requests for files with high popularity, which is consistent with the numerical results shown in Fig. 3.

V. CONCLUSION

In this letter, we have investigated the performance of a cache- and EH-assisted D2D-aided NOMA network. The performance of the underlying system has been examined in terms of OP for both the pSIC and ipSIC scenarios with/without wireless caching. In addition, we also analyzed the cache hit probability and asymptotic behavior of OP to provide useful insights into the achievable diversity order. Our results have revealed the superiority of the CA scheme over its CF counterpart, and have further demonstrated its effectiveness to overcome the bottleneck of energy and spectral constraints for the D2D-aided NOMA network.

ACKNOWLEDGMENT

This work was supported in part by the Research Council of Finland (former Academy of Finland) through EnergyNet Fellowship under Grants 321265, 328869, and 352654, and through X-SDEN Project under Grant 349965, in part by JAES Foundation through STREAM Project, in part by the NRF of South Africa through BRICS Multilateral Research and Development Project under Grant 116018, and in part by the Centre for Telecommunication Access (CeTAS) through the Telkom Centre of Excellence (CoE) Program.

REFERENCES

[1] Z. Zhao, M. Xu, W. Xie, Z. Ding, and G. K. Karagiannidis, "Coverage performance of NOMA in wireless caching networks," *IEEE Commun. Lett.*, vol. 22, no. 7, pp. 1458–1461, Jul. 2018.

[2] Z. Ding, P. Fan, G. K. Karagiannidis, R. Schober, and H. V. Poor, "NOMA assisted wireless caching: Strategies and performance analysis," *IEEE Trans. Commun.*, vol. 66, no. 10, pp. 4854–4876, Oct. 2018.

[3] Y. Meng, Z. Zhang, and Y. Huang, "Cache- and energy harvesting-enabled D2D cellular network: Modeling, analysis and optimization," *IEEE Trans. Green Commun. Netw.*, vol. 5, no. 2, pp. 703–713, Jun. 2021.

[4] S. Gautam, T. X. Vu, S. Chatzinotas, and B. Ottersten, "Cache-aided simultaneous wireless information and power transfer (SWIPT) with relay selection," *IEEE J. Sel. Areas Commun.*, vol. 37, no. 1, pp. 187–201, Jan. 2019.

[5] Y. Ren, K. Qian, X. Zhang, F. Jiang, and G. Lu, "Joint power and time allocation in NOMA-SWIPT enabled wireless caching networks," in *Proc. IEEE 96th Veh. Technol. Conf.*, 2022, pp. 1–5.

[6] A. K. Shukla, K. Yadav, P. K. Upadhyay, and J. M. Moualeu, "Exploiting deep learning in the performance evaluation of EH-based coordinated direct and relay transmission system with cognitive NOMA," *IEEE Commun. Lett.*, vol. 27, no. 6, pp. 1501–1505, Jun. 2023.

[7] D. Wan, M. Wen, F. Ji, Y. Liu, and Y. Huang, "Cooperative NOMA systems with partial channel state information over Nakagami- *m* fading channels," *IEEE Trans. Commun.*, vol. 66, no. 3, pp. 947–958, Mar. 2018.

[8] M. F. Kader, S. M. R. Islam, and O. A. Dobre, "Device-to-device aided cooperative NOMA transmission exploiting overheard signal," *IEEE Trans Wireless Commun.*, vol. 21, no. 2, pp. 1304–1318, Feb. 2022.

[9] A. Jee, K. Agrawal, and S. Prakriya, "A coordinated direct AF/DF relay-aided NOMA framework for low-outage," *IEEE Trans. Commun.*, vol. 70, no. 3, pp. 1559–1579, Mar. 2022.

[10] V. Singh et al., "On the performance of cache-free/cache-aided STBC-NOMA in cognitive hybrid satellite-terrestrial networks," *IEEE Wireless Commun. Lett.*, vol. 11, no. 12, pp. 2655–2659, Dec. 2022.

[11] G. K. Pandey, D. S. Gurjar, S. Yadav, and S. Solanki, "UAV-empowered IoT network with hardware impairments and shadowing," *IEEE Sensors Lett.*, vol. 7, no. 7, Jul. 2023, Art. no. 7500404.

[12] X. Zhou, R. Zhang, and C. K. Ho, "Wireless information and power transfer: Architecture design and rate-energy tradeoff," *IEEE Trans. Commun.*, vol. 61, no. 11, pp. 4754–4767, Nov. 2013.

[13] T. Schenk, *RF Imperfections in High-Rate Wireless Systems: Impact and Digital Compensation*. Berlin, Germany: Springer, 2008.

[14] I. S. Gradshteyn and I. M. Ryzhik, *Tables of Integrals, Series and Products*, 6th ed. San Francisco, CA, USA: Academic, 2000.

[15] M. Abramowitz and I. A. Stegun, *Handbook of Mathematical Functions with Formulas, Graphs, and Mathematical Tables*. New York, NY, USA: NBS Pub., 1972.